Scientific Research Publishing

International Journal of Geosciences, 2022, 13, 882-904
https://www.scirp.org/journal/ijg
ISSN Online: 2156-8367
ISSN Print: 2156-8359

Structural and Chemical Characteristic of Tourmaline, and Mineralogy of Associated Micas from Tourmaline Bearing Quartzite of Kombé II (Bafia Group, Central Africa Fold Belt); Implication on the Metamorphic Conditions

Ganwa Alembert Alexandre[1,2*], Klötzli Urs[2], Tchakounté Numbem Jacqueline[3], Klötzli Eva[2], Ertl Andreas[4], Djom Bernard[3]

[1]Department of Earth Sciences, University of Ngaoundéré, Ngaoundéré, Cameroon
[2]Department of Lithospheric Research, University of Vienna, Vienna, Austria
[3]Department of Earth Sciences, University of Yaoundé I, Yaoundé, Cameroon
[4]Institut Für Mineralogie und Kristallographie, University of Vienna, Vienna, Austria
Email: *ganwa1@yahoo.fr

How to cite this paper: Alexandre, G.A., Urs, K., Jacqueline, T.N., Eva, K., Andreas, E. and Bernard, D. (2022) Structural and Chemical Characteristic of Tourmaline, and Mineralogy of Associated Micas from Tourmaline Bearing Quartzite of Kombé II (Bafia Group, Central Africa Fold Belt); Implication on the Metamorphic Conditions. *International Journal of Geosciences*, **13**, 882-904.
https://doi.org/10.4236/ijg.2022.1310044

Received: June 29, 2022
Accepted: October 21, 2022
Published: October 24, 2022

Abstract

Bafia Group is part of the southernmost portion of the Central African Fold Belt (CAFB) in Cameroon. The geological feature of the group is characterized by the presence of metamorphic rocks in which tourmaline had been recognized among accessory minerals. In the present study, attention is focus on the tourmaline bearing quartzite to the southeast of Kombé II. Structure refinement shows that tourmaline is a Fe-dravite with the formula $X(Na_{0.95}[]_{0.05})Y(Mg_{2.39}Fe_{0.61})Z(Al_{5.10}Mg_{0.90})(BO_3)_3T[Si_6O_{18}](OH)_3[(O,OH)_{0.88}F_{0.12}]$. The Fe-dravite is hosted in a Ca-poor quartzite, which is made up, in addition to quartz and tourmaline, of biotite and muscovite. The structure of the dravites shows a low vacancy at the X site, which militates for a crystallization of the tourmaline at a high temperature > 750˚C. This is in agreement with previous work which shows that the metamorphic peak in the associated biotite gneiss reaches 825˚C. The R1 value of 1.24% means that the crystal structure of the tourmalines is of high quality. The genetical link between gold mineralization and tourmaline should stimulate exploration interest in the study area.

Keywords

Fe-Dravite, Structure Refinement, Accessory Mineral, Metamorphic

Condition, Kombé II, Bafia Group, Central African Fold Belt

1. Introduction

Tourmaline is an accessory mineral usually present in a large variety of rocks: sedimentary, metamorphic, plutonic rocks and their hydrothermal aureoles. The wide range of possibility of tourmaline appearance makes it a good candidate as a petrogenetic indicator ([1] [2] [3]). Despite this ubiquity of tourmaline, tourmaline rich rocks or tourmalinites are very rare. It is even suggested that rocks with more than 15 vol% tourmaline are enigmatic ([4]).

In the Bafia Group of the Cameroonian portion of the Central African Fold Belt (CAFB), tourmaline has been described as an accessory mineral in metamorphic rocks ([5] [6] [7]). Tourmaline bearing quartzite has been mentioned for the first time in Kombé II by [5] Ganwa (1998). In this paper focusing on the tourmaline bearing quartzite, we refine the structure of the tourmaline variety dravite, report the chemical composition thereof and of associated micas (muscovite and biotite), in order to determine qualities of tourmaline crystal and its implications on metamorphic conditions.

2. Geological Setting

The Kombé II area belongs to the Bafia group which is considered as the southernmost termination of the Adamawa-Yadé Domain (ADY) of the Central Africa Fold Belt (CAFB) in Cameroon ([8] [9]) and which has been recently considered as a piece of Archaean/Palaeoproterozoic crust detached from the Congo craton in the early Neoproterozoic times ([10]) (**Figure 1**). It has been described as a Neoproterozoic immature sedimentary sequence, with detritus of various sources (Archean, Paleoproterozoic, Mesoproterozoic, [8] [9]) associated with orthogneisses of Paleoproterpzoic ages ([11] [12]). The Bafia area is made up of metamorphic rocks, mainly gneisses, amphibolites, micaschists and quartzites ([5] [6]). Gneisses have various compositions (amphibole-biotite gneiss, garnet-biotite gneiss, biotite gneiss) with intercalation of amphibolites, micaschists and quartzites. Formerly, the Bafia Group was known under the name of Bafia series and formed with the Yaoundé series the Groupe of Yaoundé ([13]). Since the studies carried out by [5] [6] [8] [9] [14], Bafia series is denominated as a specific litho-structural group as a whole. The particularity of the Bafia group with respect to the other areas of the ADY in Cameroon is the NNE-SSW stretching structures, regionally highlight by hill chains with ridge lines underlain by quartzite, and the occurrence of Pan-African meta-plutonites ([5] [7] [9]). Quartzites are either pure quartzites or minerals bearing quartzites such as two micas quartzite, muscovite quartzite, garnet quartzite and tourmaline quartzite ([5]). Pure quartzite is located at the top of the hills (**Figure 2**) where it is interleaved with mica-schist. Due to differential weathering huge blocks of

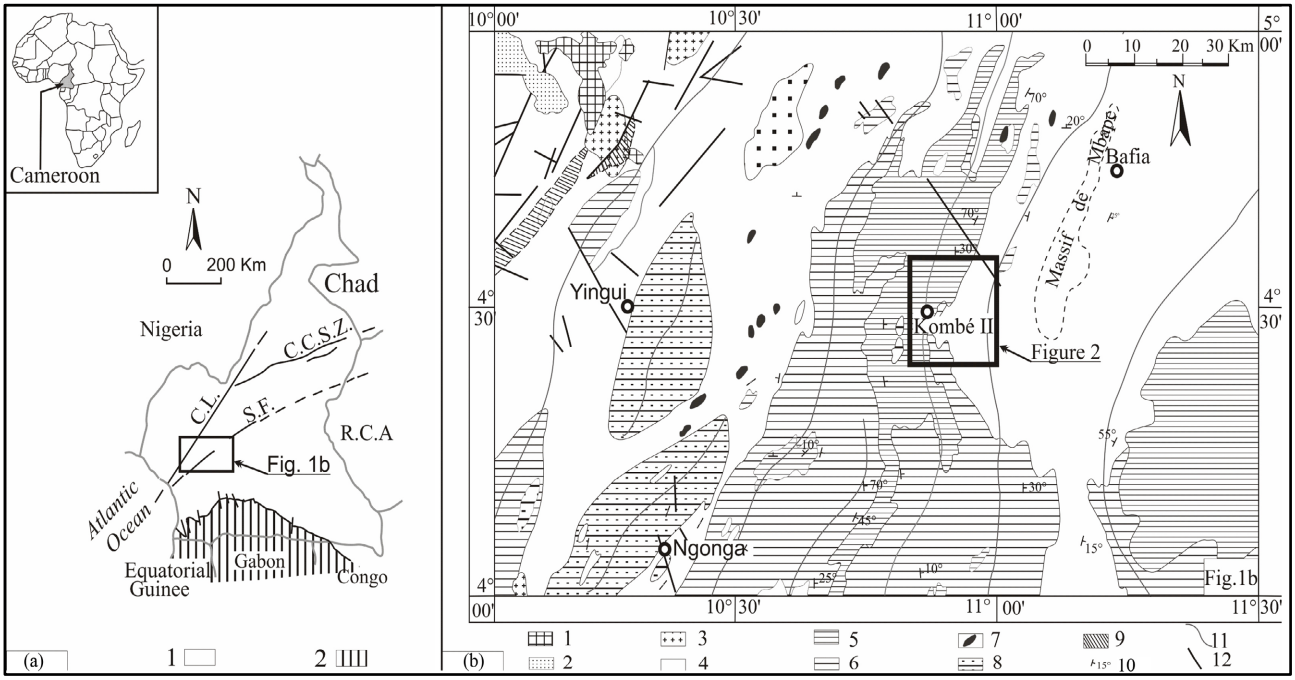

Figure 1. (a): Position of the Bafia area in the Pan-African fold belt of Cameroon. 1: Pan-African domain; 2: Northern edge of Congo craton; CL: Cameroon line; SF: Sanaga Fault; CCSZ: "Central Cameroonian Shear Zone". (b): Geological sketch map of the Bafia area (modified after Weecksteen (1957), Dumort (1968)) showing the KombéII area. 1: Tertiary volcanism; 2: Cretaceous sediments; 3: Granite; 4: Mica-schist and quartzite; 5: Undifferentiated gneisses; 6: Amphibolites, pyroxenites; 7: Granulites, 9: Mylonite; 10: Strike and dip; 11: Tectonic line, 12 Faults.

quartzite are not in place, some of which are fold hinges (**Figure 3(a)**); sometime, blocks of quartzite are supported by small portions of mica-schist, forming a type of "hoodoo" structure (chéminée de fée) (**Figure 3(b)**). Quartzite rich in tourmaline has been reported for the first time in the Bafia group to the East of the Kombé II village at Lilpagang by Ganwa [5] (**Figure 2**).

3. Analytical Methods

The tourmaline bearing quartzites were investigated by optical polarizing microscopy and back-scattered electron (BSE) imaging using a Fei INSPECT S50 (Department of Lithospheric Research, University of Vienna). The mineral chemistry was established using a CAMECA SX-100 electron microprobe (Department of Lithospheric Research, University of Vienna). The conditions of operation were: 15 kV accelerating voltage, 20 nA beam current, 20 s counting time on peak position, and a PAP correction procedure for data reduction. Analyses were carried out with a defocused 5 μm electron beam, minimizing the loss of Na and K. Calibration was based on the following standards: quartz (Si), corundum (Al) albite (Na), olivine (Mg), almandine (Fe), wollastonite (Ca), rutile (Ti), spessartine (Mn), orthoclase (K), Mg-chromite (Cr) and Ni-oxide (Ni).

For the crystallographic characterization tourmaline was mounted on a Bruker Apex CCD diffractometer equipped with graphite-monochromated Mo*Ka* radiation at the "Institut für Mineralogie und Kristallographie, Geozentrum,

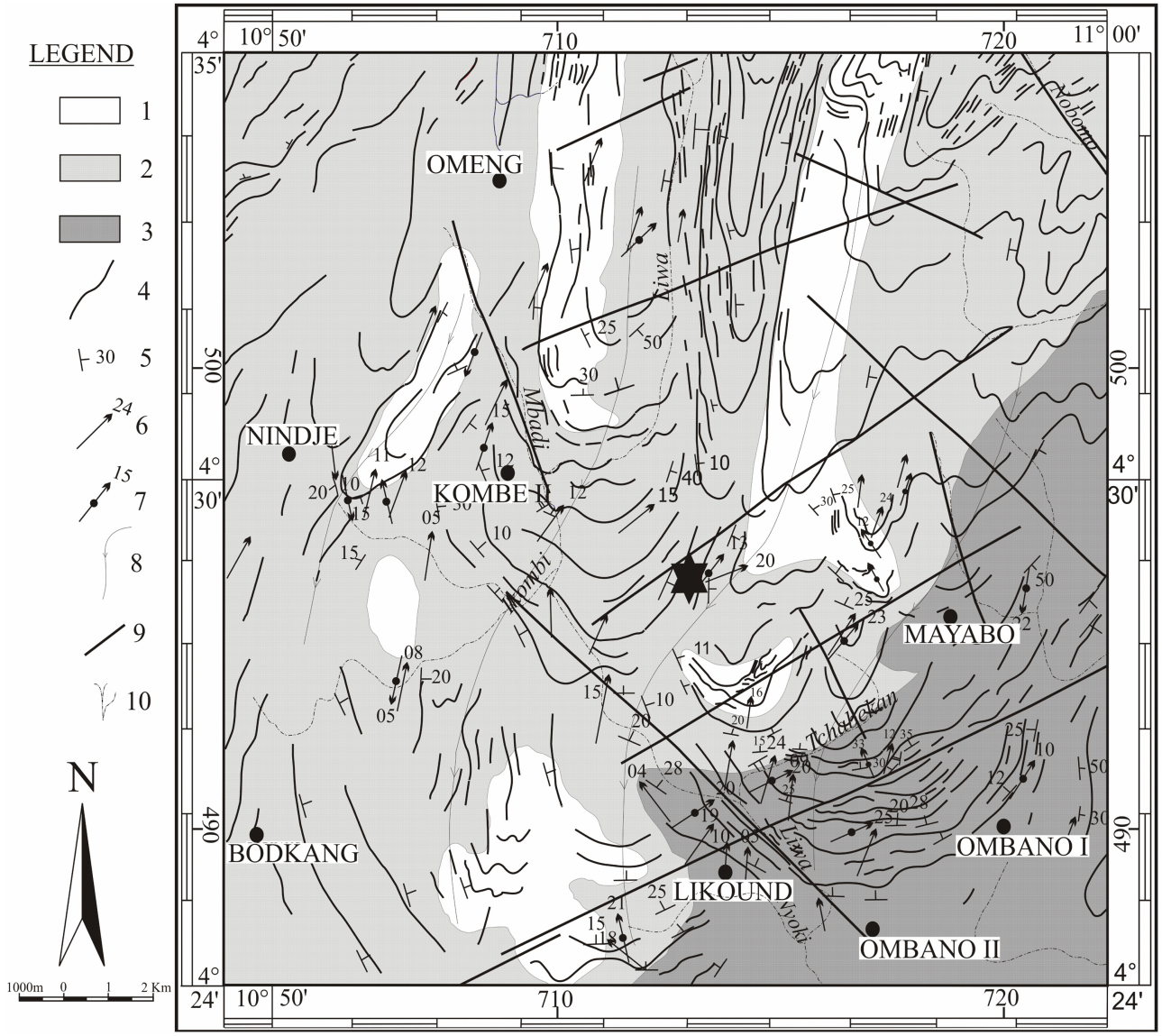

Figure 2. Geological map of the Kombé II area ([5]), showing the location of the tourmaline bearing quartzite (Black star) 1: Quartzite; 2: Garnet biotite gneiss with intercalation of amphibolite and garnet amphibole gneiss; 3: Biotite muscovite gneiss; 4: Trajectory of S1 foliation; 5: Strike and dip of S1; 6: L2 lineation; 7: Axis of F2 folds; 8: Trajectory of thrusting; 9: Fractures; 10: Rivers.

Universität Wien. Redundant data were collected for an approximate sphere of reciprocal space, and were integrated and corrected for Lorentz and polarization factors using the Bruker program SaintPlus (Bruker AXS Inc. 2001). The structure was refined using tourmaline starting models and the Bruker SHELXTL v 6.1 program package, with neutral-atom scanning factors and terms for anomalous dispersion. The structure refinement was performed with anisotropic thermal parameters for all non-hydrogen atoms.

4. Petrography of the Quartzite

At Lilpagang, quartzite outcrops are found to the South East of Kombé II village in the form of a cliff (**Figure 4**). This cliff is made up of decimetric to metric

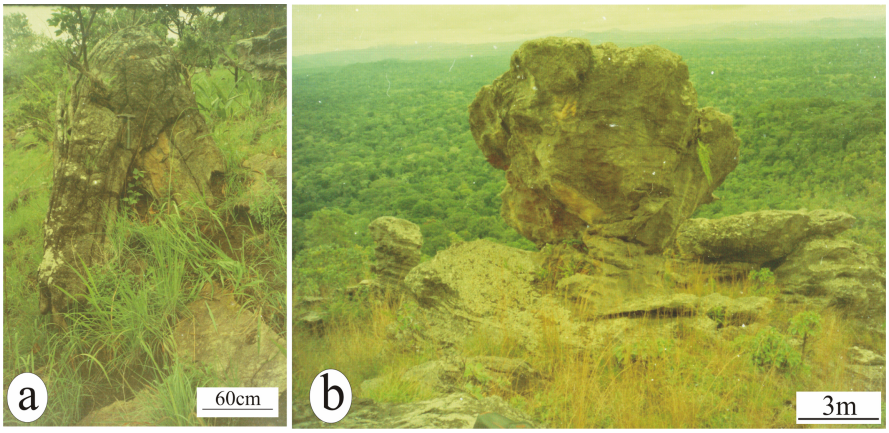

Figure 3. (a) Bloc of quartzite not in place, showing a fold hinge; (b) "hoodoo" structure forming by differential weathering between quartzite and micaschist.

Figure 4. Cliff at Lilpagang forest, made up of migmatitic biotite gneiss with intercalation of tourmaline bearing quartzite layers.

layers of tourmaline bearing quartzite, interleaved with migmatitic biotite gneiss. Quartzite and gneiss underwent ductile deformation with an S1 foliation; in the quartzite, the S1 foliation is marked by milimetric thick muscovite rich layers, which alternate with 2 to 5 cm thick quartz rich layers. Tourmaline crystals are disseminated between quartz in the quartz rich layers (**Figure 5(a)**) and also associated with muscovite in the thin mica rich layers (**Figure 5(b)**).

The whole rock geochemistry of two samples (**Table 1**) shows that tourmaline bearing quartzite is characterized by 72.04 - 73.99 wt% of SiO_2, 11.29 - 11.86 wt% Al_2O_3, 3.53 - 6.08 wt% Fe_2O_3, 3.49 - 5.78 wt% K_2O, 2.12 - 2.14 wt% Na_2O; MgO and CaO are <2 wt%, while TiO_2, MnO and P_2O_5 are <1 wt%. Trace elements Ba, Cr, Nb, Ni, Rb, Sr, V, Y, and Zr are present. Under the microscope, the quartzite layers are granoblastic and heterogranular in texture, made up of quartz (ca. 81

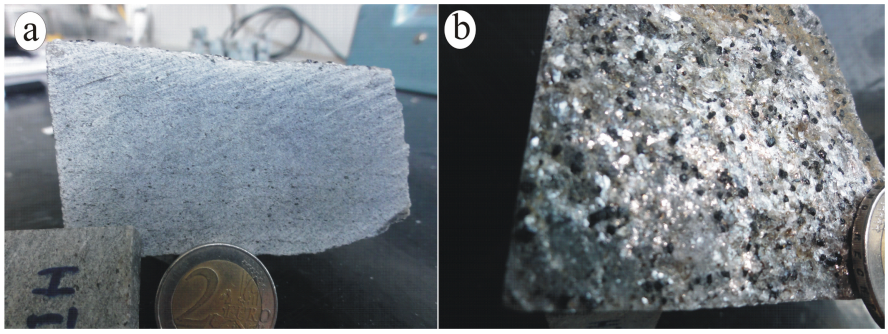

Figure 5. Tourmaline crystals disseminated in the quartz rich layer (a), and S1 Foliation surface of the tourmaline bearing quartzite showing association of tourmaline and muscovite (b).

Table 1. Whole rock chemical composition of tourmaline bearing quartzite.

Sample	HI4C	HI4S
SiO_2	73.99	72.04
TiO_2	0.34	0.49
Al_2O_3	11.86	11.29
Fe_2O_3	3.53	6.08
MnO	0.03	0.08
MgO	0.35	1.74
CaO	0.67	1.07
Na_2O	2.12	2.14
K_2O	5.78	3.49
P_2O_5	0.03	0.08
LOI	0.4	0.5
SUM	99.31	99.17
Ba	984.5	729
Cr	1	82
Nb	16.5	12
Ni	2	2
Rb	132.5	115
Sr	54.5	79
V	5	44
Y	81.5	32
Zn	58	102
Zr	674	463

vol%), muscovite (ca. 13 vol%), tourmaline (ca. 4 vol%), biotite (ca. 1.5 vol%) and chlorite (ca. 0.5 vol%). Quartz forms xenomorphic and elongated crystals of 1.9 mm length in average. Quartz often portrays undulatory extinction. Muscovite forms small anhedral crystals dispersed between quartz grains in the quartzite layers or large flake associated to biotite and tourmaline in the interlayers. Biotite flakes are smaller in size than muscovite. Tourmaline is subhedral with variable grain sizes up to 1 mm long. Small crystals are dispersed between quartz in the quartzite layers whilst large crystals are associated with muscovite and biotite in the thin micaceous layers. One should note that under microscope, tourmaline, biotite, muscovite and quartz show sharp contact between minerals; they form an assemblage of the same generation with perfect equilibrated texture (Figure 6 and Figure 7).

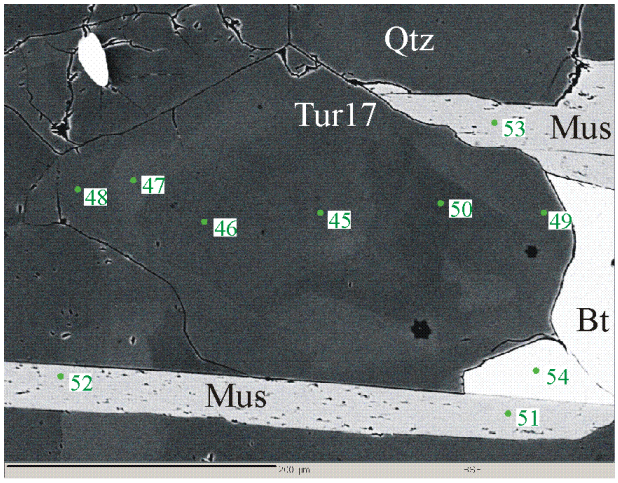

Figure 6. BSE image of the association tourmaline, muscovite, biotite, quartz, showing the data points (green dots) of the EMPA analyses. Mus: muscovite, Bt: biotite, Tur: tourmaline, Qtz; quartz. Note the crystal chemical zonation in tourmaline.

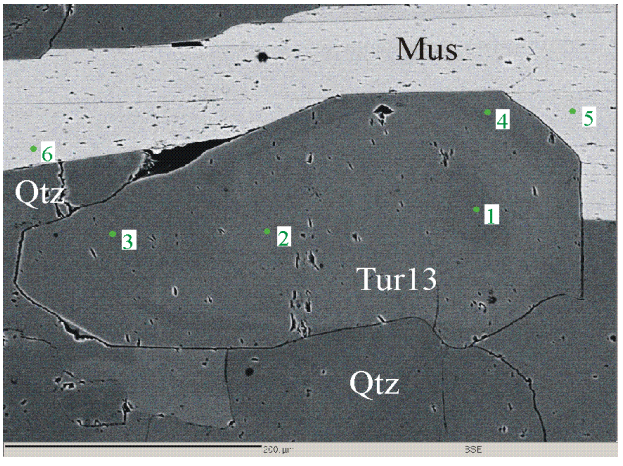

Figure 7. BSE image of the association tourmaline, muscovite, quartz, showing the data points (green dots) of the EMPA analyses. Mus: muscovite, Tur: tourmaline, Qtz; quartz.

5. Structure Refinement of Tourmaline

Structure refinements of tourmaline crystals give following values: $^{X}(Na_{0.62}Ca_{0.16}K_{0.01}\square_{0.21})$ $^{Y}(Mg_{1.20}Al_{1.20}Fe^{2+}{}_{0.54}Ti^{4+}{}_{0.06})$ $^{Z}(Al_{5.10}Mg_{0.90})$ $(BO_3)_3$ $^{T}[Si_{5.98}Al_{0.02}O_{18}]$ $(OH)_3[(OH)_{0.54}O_{0.34}F_{0.12}]$; this structure is characterized by the following lattice parameters: a = 15.946(1) Å, c = 7.197(1) Å , *R*1 = 1.24%. wR2 = 3.53%, <*X*-O> = 2.681 Å, <*Y*-O> = 2.025 Å, <*Z*-O> = 1.927 Å, <*T*-O> = 1.621 Å, <B-O> = 1.374 Å.

The studied tourmaline belongs to Fe-bearing dravite. The approximately formula is $X(Na_{0.95}[]_{0.05})Y(Mg_{2.39}Fe_{0.61})Z(Al_{5.10}Mg_{0.90})(BO_3)_3T[Si_6O_{18}](OH)_3[(O,OH)_{0.88}F_{0.12}]$. There is only a small F content and a minor vacancy (0.5 apfu) at the X site. The F content as calculated from the structure refinement is around 0.23 wt%. This is in agreement with the chemical composition of the mineral (cf. **Table 2**) which shows nil values for the F and a value of X site vacancy less than 0.3. The Mg at Z site includes also Al-The Fe is mainly Fe^{2+} and some Fe^{3+}. There is a significant disorder of Al-Mg between the Y and the Z site. There might be a tiny amount of Al at the T site. This is corroborated by the chemical analyses (cf. table) all comprises between 0.007 and 0.138 in the T site.

6. Mineralogy

6.1. Tourmaline

In BSE images tourmalines show zonation patterns that are not well organized (cf. **Figure 6**). This optical zonation is also reflected in the chemical composition of the crystal. Considering the crystal Tur17 of the **Figure 6**, one notes an increase of the Mg/(Fe + Mg) ratio from the core (data set point 45, **Table 2**) with a value of 0.794 to the rim where one has values of 0.805 (data set point 48, rim in contact with quartz) and 0.806 (data set point 50, rim in contact with biotite). The chemical composition at the rim of tourmaline crystal seems not to have been influenced by neighboring minerals as can be seen in the **Figure 7**. In fact, the dataset point 4 in contact with muscovite has a Mg/(Fe + Mg) ratio of 0.800 (**Table 2**) close similar to the ratio of data point set 3 (0.798) in contact with quartz (**Table 2**). Nevertheless, the Fe ratios vary in a very narrow interval regardless the position of the data set point in a crystal.

Principal constituents at the X-site show that the tourmalines crystals belong to the alkali subgroup (**Figure 8(a)**) of [16] Hawthorne and Henry (1999). In the corresponding diagram, two clusters of data set can be observed with ^{X}Ca less (bounded by grey rectangle) or more than 0.124. No discrimination can be observed with respect to the position of data points in the mineral grains. Inside the grey rectangle for instance, are data points from the core (7, 11, 18, 38, 45; table), data points from the rim (20; **Table 2**) and data points from intermediate domain (1, 32, 39, 42, 46, 50; table). The same observation can be made in the rest of the data. It appears that no simple zonation can be seen in respect to the position of the data point in the crystal.

Table 2. Chemical composition of tourmaline.

DataSet	1/1.	2/1.	3/1.	4/1.	7/1.	8/1.	9/1.	10/1.	11/1.	12/1.	13/1	14/1.
SiO_2	37.364	37.024	37.018	37.046	37.296	37.014	37.112	36.652	37.427	36.905	36.877	36.863
TiO_2	0.271	0.419	0.588	0.836	0.375	0.473	0.499	0.443	0.46	0.506	0.533	0.639
Al_2O_3	32..613	33.065	33.601	32.959	33.411	32.827	33.848	33.014	33.046	32.554	33.975	33.869
Cr_2O_3	0	0.01	0.004	0.035	0.003	0.029	0.011	0.007	0.008	0.008	0.01	0.005
FeO	4.139	4.056	3.868	4.022	4.2	4.304	3.78	4.028	4.19	4.166	3.697	3.782
MgO	9.208	9.005	8.567	9.031	8.592	9.15	8.53	8.91	8.818	9.136	8.542	8.522
CaO	0.629	1.299	1.099	1.101	0.537	1.108	1.053	1.294	0.551	1.149	1.006	1.065
MnO	0.004	0.018	0.004	0	0.008	0.006	0.014	0	0.002	0.003	0	0.037
Na_2O	2.181	1.813	1.986	2.07	1.985	1.93	2.049	2.007	1.926	1.882	2.009	1.828
K_2O	0.034	0.033	0.063	0.051	0.058	0.044	0.054	0.033	0.054	0.05	0.059	0.033
Total	86.442	86.742	86.797	87.149	86.464	86.885	86.95	86.385	86.484	86.359	86.706	86.644
Comment	A2_Tu017	A2_Tu017	A2_Tu017	A2_Tu017	A1_Tu006	A1_Tu006	A1_Tu006	A1_Tu006	A1_Tu010	A1_Tu010	A1_Tu010	A1_Tu010
Structural formula based on 31 anions (O, OH, F)												
T; Si	5.981	5.906	5.885	5.885	5.956	5.910	5.884	5.874	5.978	5.922	5.862	5.867
Al	0.019	0.094	0.115	0.115	0.044	0.090	0.116	0.126	0.022	0.078	0.138	0.133
B	3.000	3.000	3.000	3.000	3.000	3.000	3.000	3.000	3.000	3.000	3.000	3.000
Z; Al	6.000	6.000	6.000	6.000	6.000	6.000	6.000	6.000	6.000	6.000	6.000	6.000
Mg	0.000	0.000	0.000	0.000	0.000	0.000	0.000	0.000	0.000	0.000	0.000	0.000
Cr	0.000	0.000	0.000	0.000	0.000	0.000	0.000	0.000	0.000	0.000	0.000	0.000
Fe^{3+}	0.000	0.000	0.000	0.000	0.000	0.000	0.000	0.000	0.000	0.000	0.000	0.000
Y; Al	0.134	0.122	0.180	0.056	0.245	0.087	0.209	0.110	0.199	0.079	0.227	0.219
Ti	0.033	0.050	0.070	0.100	0.045	0.057	0.059	0.053	0.055	0.061	0.064	0.076
V	0.000	0.000	0.000	0.000	0.000	0.000	0.000	0.000	0.000	0.000	0.000	0.000
Cr	0.000	0.001	0.001	0.004	0.000	0.004	0.001	0.001	0.001	0.001	0.001	0.001
Fe^{3+}	0.000	0.000	0.000	0.000	0.000	0.000	0.000	0.000	0.000	0.000	0.000	0.000
Mg	2.197	2.141	2.030	2.139	2.046	2.178	2.016	2.129	2.100	2.185	2.024	2.022
Mn	0.001	0.002	0.001	0.000	0.001	0.001	0.002	0.000	0.000	0.000	0.000	0.005
Fe^{2+}	0.554	0.541	0.514	0.534	0.561	0.575	0.501	0.540	0.560	0.559	0.491	0.503
Zn	0.000	0.000	0.000	0.000	0.000	0.000	0.000	0.000	0.000	0.000	0.000	0.000
Li*	0.081	0.141	0.205	0.167	0.102	0.099	0.211	0.167	0.085	0.114	0.192	0.173
Total Y	3.000	3.000	3.000	3.000	3.000	3.000	3.000	3.000	3.000	3.000	3.000	3.000
X; Ca	0.108	0.222	0.187	0.187	0.092	0.190	0.179	0.222	0.094	0.198	0.171	0.182
Ba	0.000	0.000	0.000	0.000	0.000	0.000	0.000	0.000	0.000	0.000	0.000	0.000
Na	0.677	0.561	0.612	0.638	0.615	0.597	0.630	0.624	0.596	0.586	0.619	0.564
K	0.007	0.007	0.013	0.010	0.012	0.009	0.011	0.007	0.011	0.010	0.012	0.007
Rb	0.000	0.000	0.000	0.000	0.000	0.000	0.000	0.000	0.000	0.000	0.000	0.000

Continued

Cs	0.000	0.000	0.000	0.000	0.000	0.000	0.000	0.000	0.000	0.000	0.000	0.000
r	0.208	0.211	0.188	0.165	0.282	0.204	0.180	0.147	0.298	0.207	0.198	0.248
OH	4.000	4.000	4.000	4.000	4.000	4.000	4.000	4.000	4.000	4.000	4.000	4.000
F	0.000	0.000	0.000	0.000	0.000	0.000	0.000	0.000	0.000	0.000	0.000	0.000
Cl	0.000	0.000	0.000	0.000	0.000	0.000	0.000	0.000	0.000	0.000	0.000	0.000
Mg/(Fe + Mg)	0.799	0.798	0.798	0.800	0.785	0.791	0.801	0.798	0.790	0.796	0.805	0.801
Mineral Name	Dravite	Dravite	Dravite	Dravite	Dravite	Dravite	Dravite	Dravite	Dravite	Dravite	Dravite	Dravite
DataSet	18/1.	19/1.	20/1.	22/1.	23/1.	24/1.	25/1.	26/1.	31/1.	32/1.	33/1.	34/1.
SiO_2	37.551	36.837	37.449	37.373	36.924	37.061	37.007	37.029	37.27	37.389	36.985	36.791
TiO_2	0.431	0.55	0.455	0.426	0.506	0.495	0.703	0.548	0.394	0.335	0.583	0.62
Al_2O_3	33.433	33.643	32.711	33.388	33.861	32.789	33.274	32.696	33.465	33.108	33.642	33.681
Cr_2O_3	0.018	0.012	0.001	0	0.001	0.011	0	0.006	0.012	0.009	0.011	0.013
FeO	4.002	3.766	4.235	3.883	3.807	4.099	3.753	4.186	4.165	4.146	3.93	3.797
MgO	8.595	8.572	9.022	8.726	8.573	8.984	8.715	8.982	8.642	8.811	8.623	8.513
CaO	0.671	1.127	0.59	0.985	1.106	0.977	1.024	1.289	0.835	0.543	1.166	1.062
MnO	0.016	0	0.01	0	0.008	0	0.017	0.004	0.013	0.017	0.009	0.019
Na_2O	2.13	1.961	2.236	1.921	1.982	2.049	1.928	1.873	1.81	2.157	1.975	1.978
K_2O	0.067	0.056	0.062	0.051	0.059	0.045	0.03	0.03	0.052	0.051	0.08	0.073
Total	86.914	86.521	86.772	86.736	86.826	86.505	86.444	86.643	86.658	86.566	87.003	86.547
Comment	A1_Tu001	A1_Tu001	A1_Tu001	A2_Tu012	A2_Tu012	A2_Tu012	A2_Tu012	A2_Tu012	A2_Tu015	A2_Tu015	A2_Tu015	A2_Tu015
Structural formula based on 31 anions (O, OH, F)												
T; Si	5.958	5.872	5.973	5.940	5.867	5.928	5.903	5.918	5.940	5.968	5.872	5.865
Al	0.042	0.128	0.027	0.060	0.133	0.072	0.097	0.082	0.060	0.032	0.128	0.135
B	3.000	3.000	3.000	3.000	3.000	3.000	3.000	3.000	3.000	3.000	3.000	3.000
Z; Al	6.000	6.000	6.000	6.000	6.000	6.000	6.000	6.000	6.000	6.000	6.000	6.000
Mg	0.000	0.000	0.000	0.000	0.000	0.000	0.000	0.000	0.000	0.000	0.000	0.000
Cr	0.000	0.000	0.000	0.000	0.000	0.000	0.000	0.000	0.000	0.000	0.000	0.000
Fe^{3+}	0.000	0.000	0.000	0.000	0.000	0.000	0.000	0.000	0.000	0.000	0.000	0.000
Y; Al	0.210	0.193	0.123	0.193	0.208	0.110	0.158	0.077	0.225	0.196	0.166	0.194
Ti	0.051	0.066	0.055	0.051	0.060	0.060	0.084	0.066	0.047	0.040	0.070	0.074
V	0.000	0.000	0.000	0.000	0.000	0.000	0.000	0.000	0.000	0.000	0.000	0.000
Cr	0.002	0.002	0.000	0.000	0.000	0.001	0.000	0.001	0.002	0.001	0.001	0.002
Fe^{3+}	0.000	0.000	0.000	0.000	0.000	0.000	0.000	0.000	0.000	0.000	0.000	0.000
Mg	2.033	2.037	2.145	2.067	2.031	2.142	2.072	2.140	2.053	2.097	2.041	2.023
Mn	0.002	0.000	0.001	0.000	0.001	0.000	0.002	0.001	0.002	0.002	0.001	0.003
Fe^{2+}	0.531	0.502	0.565	0.516	0.506	0.548	0.501	0.560	0.555	0.553	0.522	0.506
Zn	0.000	0.000	0.000	0.000	0.000	0.000	0.000	0.000	0.000	0.000	0.000	0.000

Continued

Li*	0.170	0.201	0.111	0.172	0.194	0.138	0.182	0.156	0.116	0.110	0.199	0.198
Total Y	3.000	3.000	3.000	3.000	3.000	3.000	3.000	3.000	3.000	3.000	3.000	3.000
X; Ca	0.114	0.192	0.101	0.168	0.188	0.167	0.175	0.221	0.143	0.093	0.198	0.181
Ba	0.000	0.000	0.000	0.000	0.000	0.000	0.000	0.000	0.000	0.000	0.000	0.000
Na	0.655	0.606	0.692	0.592	0.611	0.635	0.596	0.580	0.559	0.668	0.608	0.611
K	0.014	0.011	0.013	0.010	0.012	0.009	0.006	0.006	0.011	0.010	0.016	0.015
Rb	0.000	0.000	0.000	0.000	0.000	0.000	0.000	0.000	0.000	0.000	0.000	0.000
Cs	0.000	0.000	0.000	0.000	0.000	0.000	0.000	0.000	0.000	0.000	0.000	0.000
r	0.217	0.190	0.195	0.230	0.189	0.188	0.223	0.193	0.288	0.229	0.178	0.192
OH	4.000	4.000	4.000	4.000	4.000	4.000	4.000	4.000	4.000	4.000	4.000	4.000
F	0.000	0.000	0.000	0.000	0.000	0.000	0.000	0.000	0.000	0.000	0.000	0.000
Cl	0.000	0.000	0.000	0.000	0.000	0.000	0.000	0.000	0.000	0.000	0.000	0.000
Mg/(Fe + Mg)	0.793	0.802	0.792	0.793	0.800	0.801	0.796	0.805	0.793	0.787	0.791	0.796
Mineral Name	Dravite	Dravite	Dravite	Dravite	Dravite	Dravite	Dravite	Dravite	Dravite	Dravite	Dravite	Dravite
DataSet	38/1.	39/1.	40/1.	41/1.	42/1.	45/1.	46/1.	47/1.	48/1.	49/1.	50/1.	
SiO_2	37.377	37.664	36.978	36.908	37.266	37.461	37.38	36.803	36.948	37.402	37.624	
TiO_2	0.398	0.449	0.512	0.455	0.491	0.45	0.462	0.559	0.58	0.57	0.439	
Al_2O_3	33.698	33.531	33.83	32.975	32.701	33.372	33.303	32.978	33.645	33.636	33.688	
Cr_2O_3	0.014	0.001	0	0.015	0.01	0.024	0.018	0.016	0.006	0.032	0.011	
FeO	3.88	4.147	3.778	4.096	4.184	4.016	3.973	4.168	3.687	3.741	3.702	
MgO	8.474	8.449	8.594	8.905	8.937	8.682	8.719	8.984	8.555	8.693	8.651	
CaO	0.602	0.56	1.175	1.224	0.529	0.729	0.53	1.349	1.036	1.074	0.522	
MnO	0.001	0	0	0.002	0.014	0.014	0.009	0	0.01	0.013	0.016	
Na_2O	2.178	1.678	2.004	1.903	2.193	2.096	2.13	1.939	1.981	1.917	2.278	
K_2O	0.071	0.08	0.059	0.053	0.056	0.072	0.075	0.068	0.052	0.058	0.053	
Total	86.694	86.559	86.916	86.536	86.381	86.914	86.599	86.862	86.5	87.138	86.984	
Comment	A2_Tu016	A2_Tu016	A2_Tu016	A2_Tu016	A2_Tu016	A2_Tu013	A2_Tu013	A2_Tu013	A2_Tu013	A2_Tu013	A2_Tu013	
Structural formula based on 31 anions (O, OH, F)												
T; Si	5.939	5.993	5.867	5.903	5.968	5.948	5.956	5.873	5.886	5.914	5.953	
Al	0.061	0.007	0.133	0.097	0.032	0.052	0.044	0.127	0.114	0.086	0.047	
B	3.000	3.000	3.000	3.000	3.000	3.000	3.000	3.000	3.000	3.000	3.000	
Z; Al	6.000	6.000	6.000	6.000	6.000	6.000	6.000	6.000	6.000	6.000	6.000	
Mg	0.000	0.000	0.000	0.000	0.000	0.000	0.000	0.000	0.000	0.000	0.000	
Cr	0.000	0.000	0.000	0.000	0.000	0.000	0.000	0.000	0.000	0.000	0.000	
Fe^{3+}	0.000	0.000	0.000	0.000	0.000	0.000	0.000	0.000	0.000	0.000	0.000	
Y; Al	0.250	0.282	0.194	0.119	0.141	0.193	0.209	0.076	0.202	0.183	0.234	
Ti	0.048	0.054	0.061	0.055	0.059	0.054	0.055	0.067	0.069	0.068	0.052	

Continued

V	0.000	0.000	0.000	0.000	0.000	0.000	0.000	0.000	0.000	0.000	0.000
Cr	0.002	0.000	0.000	0.002	0.001	0.003	0.002	0.002	0.001	0.004	0.001
Fe^{3+}	0.000	0.000	0.000	0.000	0.000	0.000	0.000	0.000	0.000	0.000	0.000
Mg	2.007	2.004	2.033	2.123	2.134	2.055	2.071	2.137	2.032	2.049	2.040
Mn	0.000	0.000	0.000	0.000	0.002	0.002	0.001	0.000	0.001	0.002	0.002
Fe^{2+}	0.516	0.552	0.501	0.548	0.560	0.533	0.529	0.556	0.491	0.495	0.490
Zn	0.000	0.000	0.000	0.000	0.000	0.000	0.000	0.000	0.000	0.000	0.000
Li*	0.177	0.108	0.211	0.153	0.103	0.160	0.132	0.161	0.204	0.200	0.179
Total Y	3.000	3.000	3.000	3.000	3.000	3.000	3.000	3.000	3.000	3.000	3.000
X; Ca	0.102	0.095	0.200	0.210	0.091	0.124	0.090	0.231	0.177	0.182	0.088
Ba	0.000	0.000	0.000	0.000	0.000	0.000	0.000	0.000	0.000	0.000	0.000
Na	0.671	0.518	0.617	0.590	0.681	0.645	0.658	0.600	0.612	0.588	0.699
K	0.014	0.016	0.012	0.011	0.011	0.015	0.015	0.014	0.011	0.012	0.011
Rb	0.000	0.000	0.000	0.000	0.000	0.000	0.000	0.000	0.000	0.000	0.000
Cs	0.000	0.000	0.000	0.000	0.000	0.000	0.000	0.000	0.000	0.000	0.000
r	0.212	0.371	0.172	0.189	0.217	0.216	0.236	0.156	0.201	0.219	0.202
OH	4.000	4.000	4.000	4.000	4.000	4.000	4.000	4.000	4.000	4.000	4.000
F	0.000	0.000	0.000	0.000	0.000	0.000	0.000	0.000	0.000	0.000	0.000
Cl	0.000	0.000	0.000	0.000	0.000	0.000	0.000	0.000	0.000	0.000	0.000
Mg/(Fe + Mg)	0.796	0.784	0.802	0.795	0.792	0.794	0.796	0.793	0.805	0.806	0.806
Mineral Name	Dravite	Dravite	Dravite	Dravite	Dravite	Dravite	Dravite	Dravite	Dravite	Dravite	Dravite

The studied tourmaline crystals classify as dravite according to the classification of [15] Henry *et al*. 2002 (**Figure 8(b)**). In the classification diagram, representative points are aligned parallel to the Y axis. This arrangement reflects the variation of the vacancy + Na content (cf **Table 2**) and a constant Mg/(Mg + Fe) ratio of about 0.8. In the Al-$Fe_{(tot)}$-Mg ternary diagram ([2]), the tourmalines plot in both fields of metapelites and metapsamite coexisting with Al-saturating phase, and metapelites without an Al-saturating phase (**Figure 9(a)**). The Al-rich phase in the hosting tourmaline bearing quartzite may be the muscovite the chemistry of which shows more than 32 wt% of Al_2O_5. In the Ca-$Fe_{(tot)}$-Mg diagram the representing points are in the field of Ca-poor metapelites, metapsammites and quartz-tourmaline rocks (**Figure 9(b)**). The Ca-poor character of the host rock can be seen through its mineralogical composition made up of quartz, biotite (CaO ≤ 0.008 wt%), muscovite (CaO ≤ 0.015 wt%) tourmaline (CaO ≤ 1.35 wt%).

6.2. Biotite

Chemical composition of the analyzed biotite flakes are shown in **Table 3**; biotite

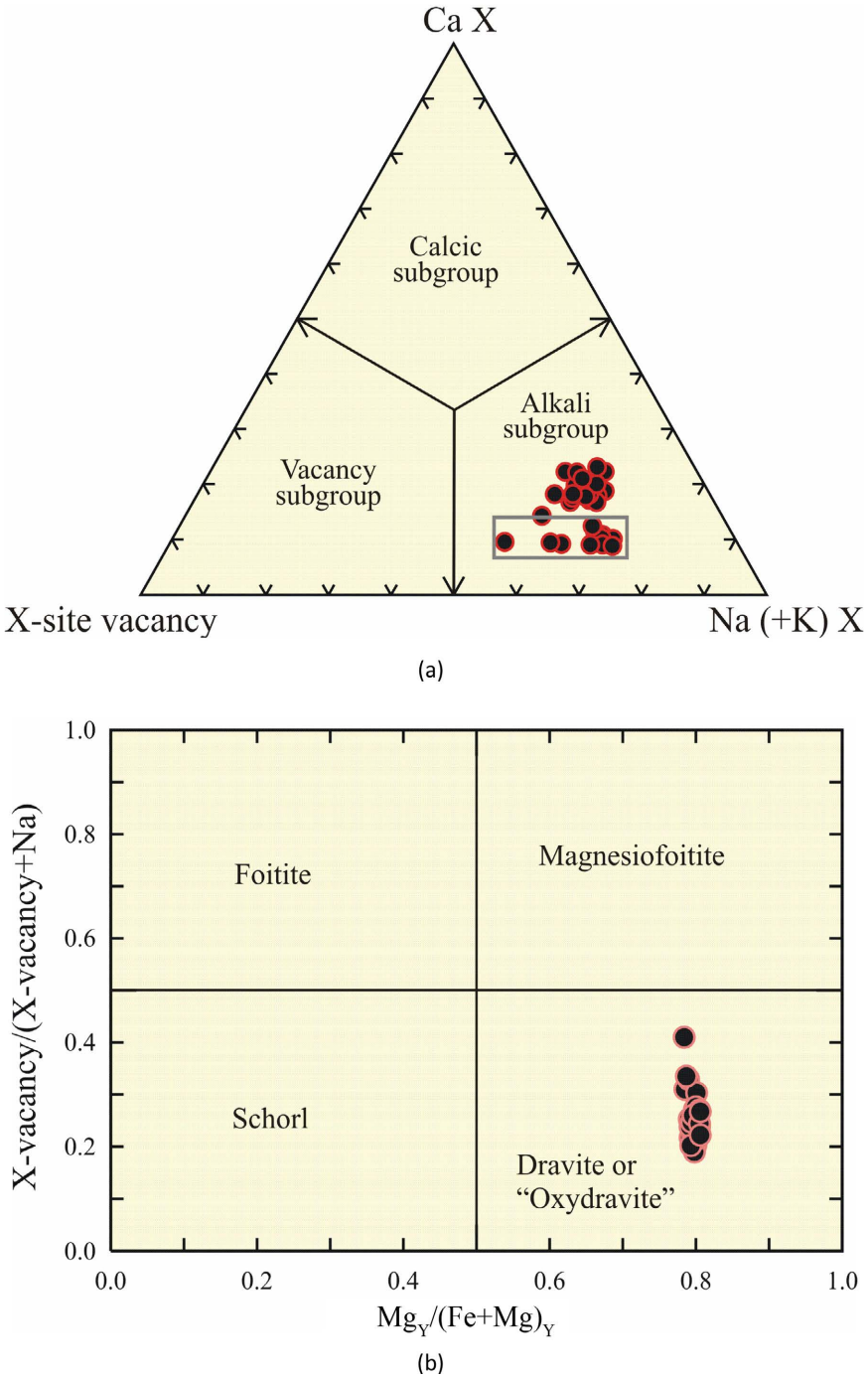

Figure 8. Classification of studied tourmaline. (a) Principal tourmaline subgroups diagram of Hawthorne and Henry ([16]): major compositional groups are defined by the principal constituents at X-site. (b) Diagram Mg/(Mg + Fe) vs /(X-vacancy/(X-vacancy + Na), according to the classification of [15].

is very poor in calcium (virtually Ca-free or equal to 0.001 apfu); There are no opaque minerals in the biotite cleavages, showing that the analyzed minerals are not affected by chloritization. The Fe/(Fe + Mg) is around 0.3 at the transition between phlogopite and biotite of [18] (**Figure 10**). In the ternary compositional

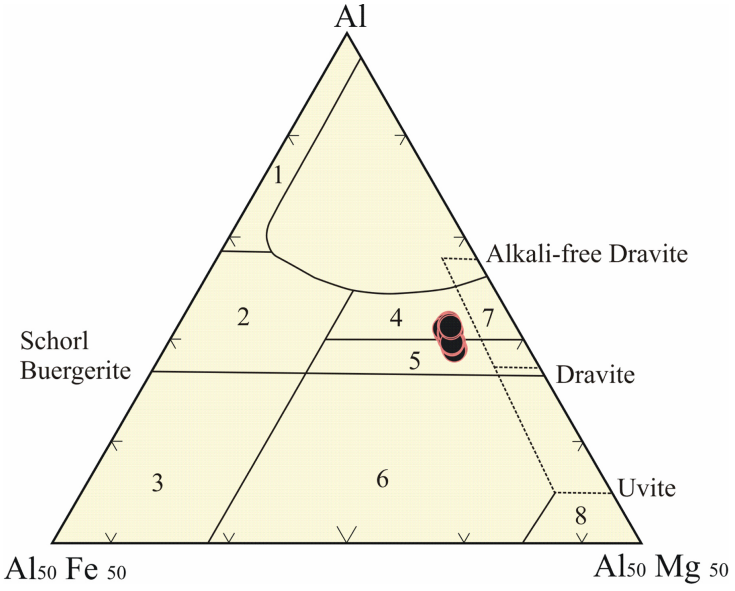

(a)

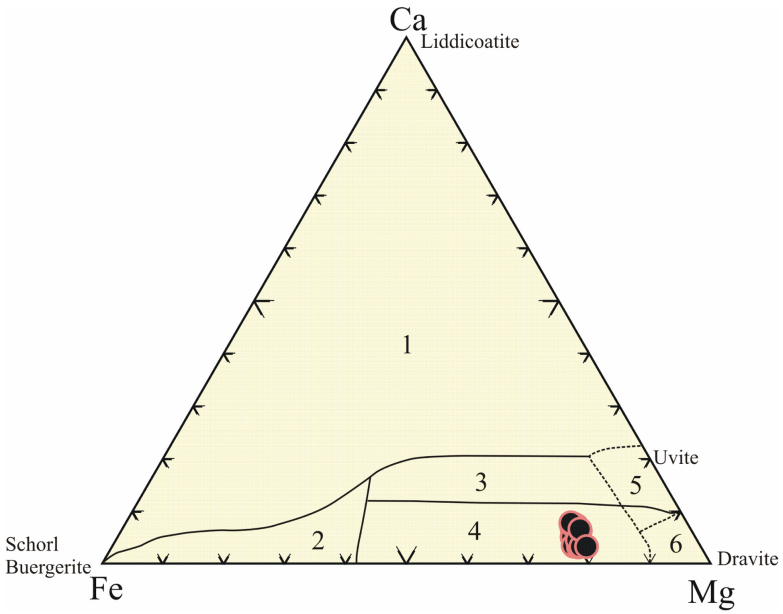

(b)

Figure 9. Tourmaline environmental diagrams of Henry and Guidotti ([2]); (a) Al-Fe(tot)-Mg diagram with numbered fields corresponding to the following rock types: (1) Li-rich granitoidpegmatites and aplites, (2) Li-poor granitoids and associated pegmatites and aplites, (3) Fe^{3+}-rich quartz-tourmaline rocks (hydrothermally altered granites), (4) Metapelites and metapsammite coexisting with an Al-saturating phase, (5) Metapelites without an Al-saturating phase, (6) Fe^{3+}-rich quartz-tourmaline rocks, calc-silicate rocks, and metapelites, (7) Low-Ca meta-ultramafics and Cr^{-}, V-rich metasediments, and (8) Meta-carbonates and meta-pyroxenites, (b) Ca-Fe(tot)-Mg diagram with the numbered fields corresponding to the following rock types: (1) Li-rich granitoidpegmatites and aplites, (2) Li-poor granitoids and associated pegmatites and aplites, (3) Ca-rich metapelites and calc-silicate rocks, (4) Ca-poor metapelites, metapsammites and quartz-tourmaline rocks, (5) Meta-carbonates, and (6) Meta-ultramafics.

Table 3. Chemical composition of biotite.

Data Set/Point	16/1.	30/1.	54/1.
SiO_2	37.536	37.623	37.497
TiO_2	1.771	1.844	2.034
Al_2O_3	17.998	18.264	18.034
FeO	11.854	11.689	12.099
MnO	0.084	0.08	0.046
MgO	15.342	15.516	15.541
CaO	0	0.005	0.008
Na_2O	0.165	0.188	0.158
K_2O	10.276	10.076	10.015
Cr_2O_3	0.003	0.045	0.021
Cl	0.008	0.026	0.019
BaO	0	0.036	0
Total	94.988	95.391	95.451
Comment	A1_Tu010	A2_Tu012	A2_Tu013
Si	5.448	5.431	5.418
Al iv	2.552	2.569	2.582
Al vi	0.527	0.539	0.490
Ti	0.193	0.200	0.221
Cr	0.000	0.000	0.000
Fe	1.439	1.411	1.462
Mn	0.010	0.010	0.006
Mg	3.319	3.339	3.348
Li*	0.713	0.723	0.703
Ca	0.000	0.001	0.001
Na	0.046	0.053	0.044
K	1.902	1.855	1.846
OH*	4.000	4.000	4.000
F	0.000	0.000	0.000
Cl	0.000	0.000	0.000
TOTAL	20.150	20.131	20.121
Y total	6.201	6.222	6.230
X total	1.949	1.909	1.891
Al total	3.079	3.108	3.072
Fe/Fe + Mg	0.302	0.297	0.304

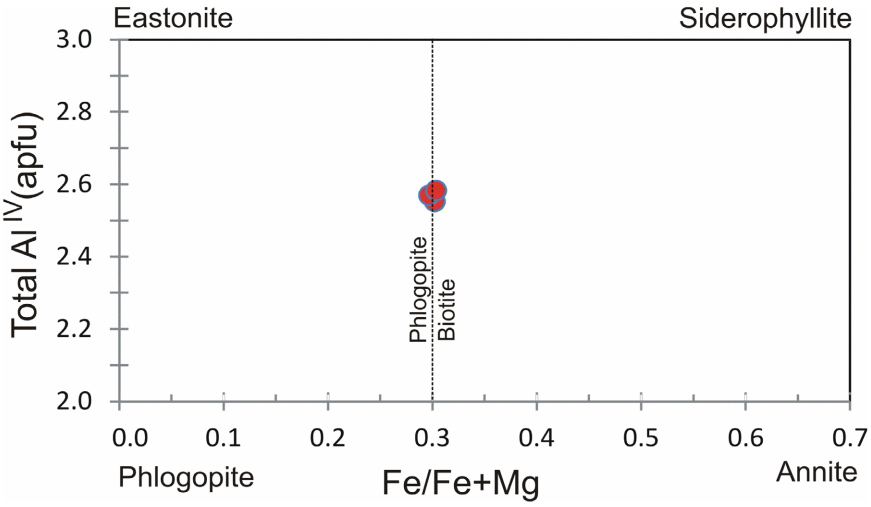

Figure 10. Classification of biotite based on [18].

system of (Al^{vi} + Fe^{3+})–Mg–(Fe^{2+} + Mn) after [19], biotite classifies as phlogopite (**Figure 11**). In the $FeO_tMgOAl_2O_3$ ternary diagram (**Figure 12**), representative points plot in the field of biotite unaccompanied by other mafic minerals [17].

6.3. Muscovite

The muscovite flakes (**Table 4**) of the tourmaline bearing quartzite exhibit the following chemical characteristic: total Al: 5.019 - 5.413 apfu, Ti: 0.072 - 0.104 apfu, Na: 0.124 - 0.175 apfu, Si: 6.136 - 6.366 apfu, Mg: 0.301 - 0.476 apfu, Mn and Cr contents are negligible. In the Mg-Ti-Na ternary diagram ([22]) the muscovites plot mainly in the field of primary muscovite. Only one data point is in the field of secondary muscovite, while few points are on the limit between the two fields (**Figure 13**). In the (Fe^{2+} + Mg) versus (Si – 6) apfu diagram (**Figure 14**) muscovites are above the muscovite-phengite solid solution. Such muscovite is classified as slightly phengitic celadonitic muscovite.

7. Discussion

The Bafia group to which belongs the Kombé II area, is considered as the southern part of the Adamawa-Yadé domain of the Pan-African Central Africa Fold Belt in Cameroon ([6] [23]). It is a meta-volcano sedimentary sequence, made up of gneisses, amphibolites and quartzites ([8] [10]). In the study area, dravite is present notably only in the quartzite layer intercalated with gneisses at the bottom of a hill at Lilpagang, while quartzites at the top of the hills are pure or muscovite-rich quartzites. The occurrence of dravite in that layer means that required conditions are met to allow the crystallization of the mineral. It means that the sedimentary protholite was sufficiently rich in alumina to allow crystallization of muscovite, and rich in boron to favour the growth of dravite. Differences of crystals size of tourmaline in the quartzite plate and in the thin muscovite rich layers can be explained by the fact that the platy micas can accommodate larger crystals than the more granular quartz. Even though the origin of the

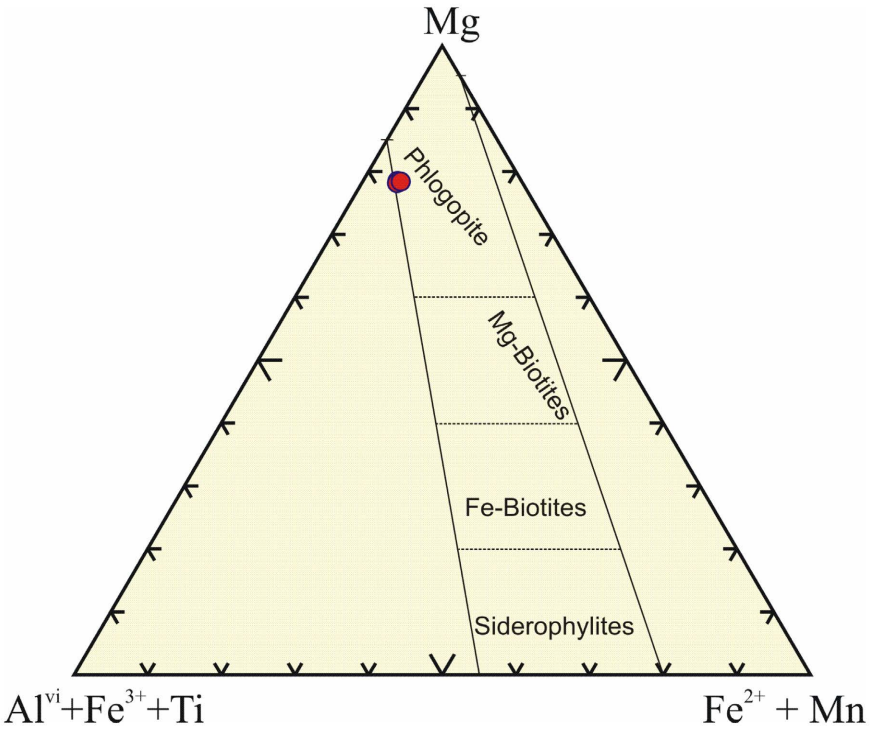

Figure 11. Plot of biotite on Foster's classification diagram [19].

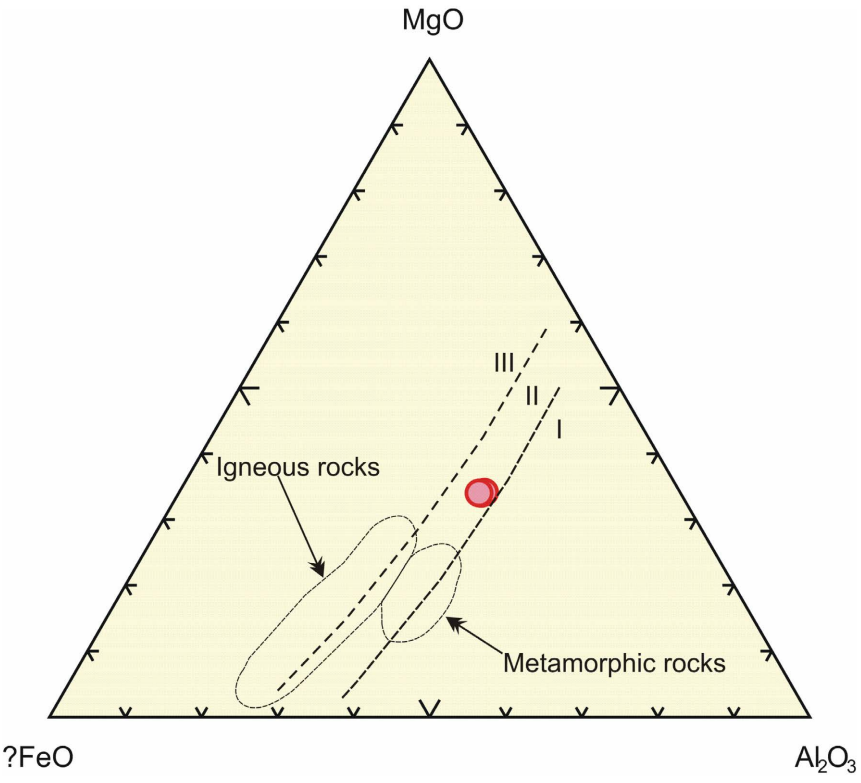

Figure 12. $FeO_tMgOAl_2O_3$ ternary plot to discriminate biotite association with mineral phases ([20]). Metamorphic and igneous fields are from [21]. I is the field of biotite associate with muscovite or topaz; II is biotite unaccompanied by other mafic minerals; and III biotite associated to amphibole, pyroxene or olivine.

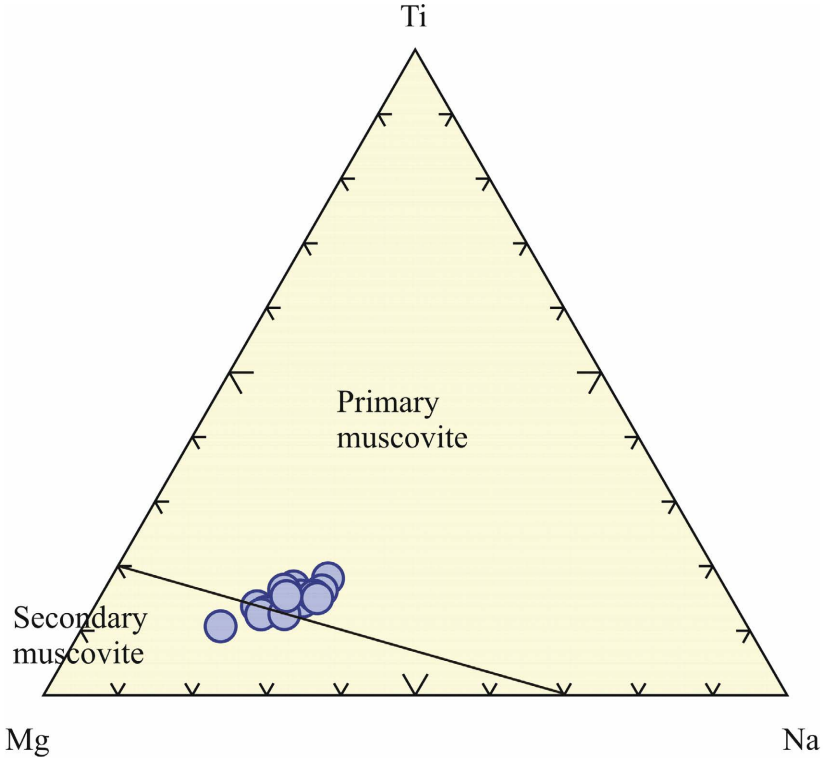

Figure 13. Ternary Mg–Ti–Na diagram for muscovite with primary and secondary fields from [22].

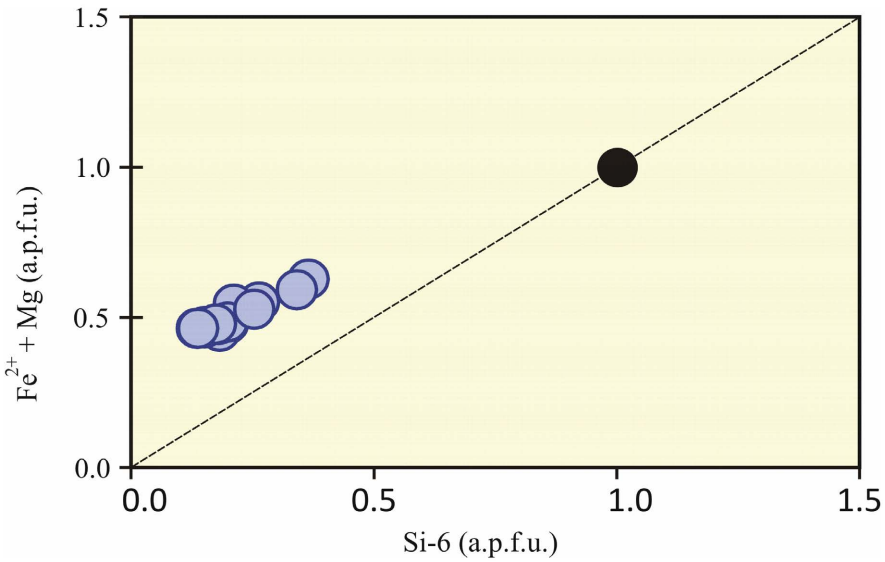

Figure 14. (Fe^{2+} + Mg) versus Si – 6 (apfu) diagram for the muscovite of the tourmaline bearing quartzite. The black circle is the phengite position whereas the ideal muscovite is positioned at the origin of the diagram: Fe^{2+}: total Fe (Fe^{2+} + Fe^{3+}).

boron is not investigated, it can be assumed that the element is transported by a fluid. This fluid can be a product of devolatisation during metamorphic process, fluid hosted in that level of the sedimentary sequence, or fluid of external origin. Furthermore, Mg/(Mg + Fe) ratios in the studied dravite rage from 0.784 to

Table 4. Chemical composition of muscovite.

DataSet	5/1.	6/1.	15/1.	17/1.	27/1.	28/1.	29/1.	35/1.	36/1.	37/1.	43/1.	44/1.
SiO_2	47.345	48.023	46.746	46.753	46.333	47.054	46.403	46.615	47.97	46.491	46.775	47.117
TiO_2	0.86	0.719	0.868	0.9	0.846	0.786	0.864	1.038	0.865	0.971	0.836	0.769
Al_2O_3	33.263	32.122	33.928	34.242	34.677	33.818	34.503	34.098	32.352	33.917	33.999	33.299
FeO	1.353	1.35	1.352	1.401	1.33	1.412	1.396	1.365	1.333	1.344	1.364	1.36
MnO	0.023	0.004	0	0.017	0.021	0.029	0	0.001	0	0	0	0.007
MgO	2.03	2.407	1.659	1.561	1.594	1.961	1.586	1.523	2.246	1.642	1.68	1.892
CaO	0.01	0.005	0.015	0.006	0.022	0.015	0.011	0.003	0	0.004	0.023	0.002
Na_2O	0.529	0.483	0.619	0.522	0.569	0.553	0.496	0.65	0.617	0.68	0.616	0.62
K_2O	10.626	10.728	10.709	10.612	10.655	10.719	10.623	10.542	10.833	10.715	10.628	10.805
Cr_2O_3	0.01	0	0.019	0.028	0.002	0.021	0.023	0	0	0.006	0.01	0.012
Cl	0.003	0	0.003	0	0	0.007	0.004	0.011	0.008	0	0	0.005
BaO	0.068	0.037	0.107	0.029	0.068	0.06	0.074	0.091	0.036	0.06	0.024	0.051
Total	96.072	95.859	96.027	96.064	96.106	96.436	95.98	95.928	96.243	95.819	95.934	95.938
Comment	A2_Tu017	A2_Tu017	A1_Tu010	A1_Tu010	A2_Tu012	A2_Tu012	A2_Tu012	A2_Tu015	A2_Tu015	A2_Tu015	A2_Tu016	A2_Tu016
Si	6.264	6.366	6.201	6.188	6.136	6.213	6.152	6.184	6.342	6.181	6.200	6.254
Al iv	1.736	1.634	1.799	1.812	1.864	1.787	1.848	1.816	1.658	1.819	1.800	1.746
Al vi	3.451	3.385	3.505	3.529	3.549	3.476	3.544	3.515	3.383	3.495	3.512	3.464
Ti	0.086	0.072	0.087	0.090	0.084	0.078	0.086	0.104	0.086	0.097	0.083	0.077
Cr	0.001	0.000	0.002	0.003	0.000	0.002	0.002	0.000	0.000	0.001	0.001	0.001
Fe	0.150	0.150	0.150	0.155	0.147	0.156	0.155	0.151	0.147	0.149	0.151	0.151
Mn	0.003	0.000	0.000	0.002	0.002	0.003	0.000	0.000	0.000	0.000	0.000	0.001
Mg	0.400	0.476	0.328	0.308	0.315	0.386	0.313	0.301	0.443	0.325	0.332	0.374
Ca	0.001	0.001	0.002	0.001	0.003	0.002	0.002	0.000	0.000	0.001	0.003	0.000
Na	0.136	0.124	0.159	0.134	0.146	0.142	0.128	0.167	0.158	0.175	0.158	0.160
K	1.793	1.814	1.812	1.791	1.800	1.805	1.796	1.784	1.827	1.817	1.797	1.829
OH*	3.999	4.000	3.999	4.000	4.000	3.998	3.999	3.998	3.998	4.000	4.000	3.999
Cl	0.001	0.000	0.001	0.000	0.000	0.002	0.001	0.002	0.002	0.000	0.000	0.001
TOTAL	18.021	18.022	18.045	18.013	18.046	18.050	18.026	18.023	18.044	18.061	18.038	18.058
Y total	4.090	4.083	4.072	4.087	4.097	4.101	4.101	4.071	4.059	4.068	4.079	4.068
X total	1.930	1.939	1.973	1.926	1.949	1.949	1.926	1.951	1.985	1.993	1.958	1.989
Al total	5.187	5.019	5.305	5.342	5.413	5.263	5.392	5.331	5.041	5.315	5.312	5.210
Fe/Fe + Mg	0.272	0.239	0.314	0.335	0.319	0.288	0.331	0.335	0.250	0.315	0.313	0.287

0.805 (cf **Table 2**), which is in the range of the value (0.4 - 1.0) determine by [24] for metamorphic tourmaline. The metamorphic origin of tourmaline is confirmed by its presence in the metamorphic mineral assemblage biotite-muscovite-tourmaline-quartz) showing a perfect equilibrated metamorphic texture (cf **Figure 6** and **Figure 7**). References [25] and [26] used FeO/(FeO + MgO) ration in tourmaline as indicator of source environments. As demonstrated by many authors working on tourmaline ([27] [28]) the composition of the studied dravite seems to be influenced by the composition of the host rock. This can be deduced from the mineralogy of the tourmaline bearing quartzite made up for example of Ca poor minerals (biotite, muscovite, quartz), hosting dravite with Ca content equal or less than 1.35 weigh percent. The values for vacancy + Na vary from 0.900 to 0.771. Na varies from 0.699 apfu to 0.518 apfu with the corresponding vacancy of 0.202 apfu and 0.371 apfu. Even though 0.202 is not the lowest value of the vacancy, globally, the Na apfu value decreases with the increase of the vacancy. The variation of the vacancy +Na could be link with the optical zonation of the tourmaline crystals; as one can see in **Figure 6**, data points 45 to 50 are localized in different domains of the tourmaline crystal and they show different values of Na apfu and vacancy (cf **Table 2**).

The structure of the dravites shows a low vacancy at the X site, which militates for a crystallization of the tourmaline at a high temperature of more than 750˚C. One should note that the layer of tourmaline bearing quartzite is intercalated with the biotite gneisses which show partial melting phenomena ([5]). This is in good agreement with the above temperature. Ganwa ([5]) shows that metamorphic path in the area reaches a possible temperature peak at 825˚C. Nevertheless, even though the presence of Al in the T site and the low F content are not favorable for the high temperature of crystallization of the tourmaline, it is likely that the studied tourmaline crystallized at about 750˚C. It is likely that tourmaline start to crystallize at the end of the granulite facies overprinting, especially during the anatexis in the adjoining gneisses. This temperature should be favorable for the production and expulsion of boron rich metamorphic fluid in the quartzite layer, or the circulation of and external boron rich fluid in the quartzite layer. The present study should lead to metallogenic research in the study area. The R1 value of 1.24% means that the crystal structure of the tourmalines is of high quality. It has been shown that gold mineralization and tourmaline are genetically linked ([29] and [30] suggest that recognition of tourmaline "should stimulate exploration interest in any area in which they occur". It has been demonstrated in the Tsa Da Glisza prospect in Yukong territory (Canada) that tourmaline has potential as an indicator mineral for emerald mineralization ([27]).

8. Conclusion

In addition to the quartzite underlining the hills summit in the Bafia Group, one has tourmaline quartzite as centimetric to decametric layers interleave with gneiss to the East of Kombé II. Studied tourmaline is belonging to the alkali

subgroup, especially Fe-bearing dravite, and is associated to phlogopite and phengitic celadonitic muscovite. These crystals are of high quality, forming at high temperature during the migmatisation of the gneiss.

Acknowledgements

The first author is great full to the association of youth of Kombé II, and especially to Bassinha Bonaventure, a hunter who guided the first author to outcrops in the forest. Laboratory analyses related to the present work have been carried out during the post-doctoral research of the first author at the University of Vienna, funded by the Austrian Science Fund FWF, project M 1371-N19. We thank Claudia, Franz Biedermann of the University of Vienna for technical assistance.

Conflicts of Interest

The authors declare no conflicts of interest regarding the publication of this paper.

References

[1] Shearer, C.K., Papike, J.J., Simon, S.B., Laul, J.C. and Christian, R.P. (1984) Pegmatite/Wallrock Interactions, Black Hills, South Dakota: Progressive Boron Metasomatism Adjacent to the Tip Top Pegmatite. *Geochimica et Cosmochimica Acta*, **48**, 2563-2579. https://doi.org/10.1016/0016-7037(84)90306-5

[2] Henry, D.J. and Guidotti, C.V. (1985) Tourmaline as a Petrogenetic Indicator Mineral: An Example from the Staurolite-Grade Metapelites of NW Maine. *American Mineralogist*, **70**, 1-15.

[3] Jolliff, B.L., Papike, J.J., Shearer, C.K. and Laul, J.C. (1986) Tourmaline as a Recorder of Pegmatite Evolution: Bob Ingersoll Pegmatite, Black Hills, South Dakota. *American Mineralogist*, **71**, 472-500.

[4] Bone, Y. (1988) The Geological Setting of Tourmalinite at Rum Jungle, N.T., Australia: Genetic and Economic Implications. *Mineralium Deposita*, **23**, 34-41. https://doi.org/10.1007/BF00204226

[5] Ganwa, A.A. (1998) Contribution à l'étude géologique de la région de Kombé II-Mayabo dans la série panafricaine de Bafia: Géomorphologie structurale, Tectonique, Pétrologie. Thèse 3ème Cycle, University of Yaoundé I, Yaoundé, 173 p. + appendices.

[6] Tchakounte, J. (1999) Etude géologique de la région d'Etoundou-Bayomen dans la série métamorphique de Bafia: Tectonique, géochimie et métamorphisme. Thèse de 3e cycle, université Yaoundé-1, Yaoundé, 190 p.

[7] Mvondo Ondoa, J. (2009) Caractérisation des évènements tectoniques dans le domaine Sud de la chaine Panafricaine au Cameroun: Styles tectoniques et géochronologiques des séries de Yaoundé et Bafia. Unpublished Ph.D. Thesis, University of Yaoundé I, Yaoundé, 186 p.

[8] Ganwa, A.A., Frisch, W., Siebel, W., Shang Kongnyuy, C., Mvondo Ondoa, J., *et al.* (2008) Zircon 207Pb/206Pb Evaporation Ages of Panafrican Metasedimentary Rocks in the Kombé-II Area (Bafia Group, Cameroon): Constraints on Protolith Age and Provenance. *Journal of African Earth Sciences*, **51**, 77-88.

https://doi.org/10.1016/j.jafrearsci.2007.12.003

[9] Tchakounté Numbem, J., Toteu, S.F., Van Schmus, W.R., Penaye, J., Deloule, E., Mvondo Ondoua, J., Bouyo Houketchang, M., Ganwa, A.A. and White, W.M. (2007) Evidence of ca 1.6-Ga Detrital Zircon in the Bafia Group (Cameroon): Implication for the Chronostratigraphy of the Pan-African Belt North of the Congo Craton. *Comptes Rendus Geoscience*, **339**, 132-142. https://doi.org/10.1016/j.crte.2007.01.004

[10] Tchakounté, J., Eglinger, A., Toteu, S.F., Zeh, A., Nkoumbou, C., Mvondo-Ondoa, J., Penaye, J., de Wit, M. and Barbey, P. (2017) The Adamawa-Yadé Domain, a Piece of Archaean Crust in the Neoproterozoic Central African Orogenic Belt (Bafia Area, Cameroon). *Precambrian Research*, **299**, 210-229. https://doi.org/10.1016/j.precamres.2017.07.001

[11] Toteu, S.F., Van Schmus, W.R., Penaye, J. and Michard, A. (2001) New U-Pb and Sm-Nd Data from North-Central Cameroon and Its Bearing on the pre-Pan-African History of Central Africa. *Precambrian Research*, **108**, 45-73. https://doi.org/10.1016/S0301-9268(00)00149-2

[12] Tanko Njiosseu, E.L., Nzenti, J.P., Njanko, T., Kapajika, B. and Nédélec, A. (2005) New U-Pb Zircon Ages from Tonga (Cameroon): Coexisting Eburnean-Transamazonian (2.1 Ga) and Pan-African (0.6 Ga) Imprints. *Comptes Rendus Geoscience*, **337**, 45-73. https://doi.org/10.1016/j.crte.2005.02.005

[13] Bessoles, B. and Trompette, M. (1980) Géologie de l'Afrique: La chaîne Panafricaine, Zone mobile d'Afrique Centrale (partie Sud) et Zone Mobile Soudanaise. Mem. B.R.G.M., Orléans? France, No. 92, 396 p., 118 fig., 26 tabl. index, bibl. (20 p).

[14] Noizet, G. (1982) Disposition géologique des régions de Yaoundé et Bafia, Ann. Fac. Sci. Yaoundé.

[15] Henry, D.J., Viator, D. and Dutrow, B.L. (2002) Estimation of Light Element Concentrations in Tourmaline: How Accurate Can It Be? Programme with Abstracts of the 18th International Mineralogical Association, 209.

[16] Hawthorne, F.C. and Henry, D.J. (1999) Classification of the Minerals of the Tourmaline Group. *European Journal of Mineralogy*, **11**, 201-215. https://doi.org/10.1127/ejm/11/2/0201

[17] Mian, I. and Le Bas, M.J. (1987) The Biotite-Phlogopite Series in Fenites from the Loe Shilman Carbonatite Complex, NW Pakistan. *Mineralogical Magazine*, **51**, 397-408. https://doi.org/10.1180/minmag.1987.051.361.06

[18] Deer, W.A., Howie, R.A. and Zussman, J. (1992) An Introduction to the Rock-Forming Minerals. 2nd Edition, Longman, London, 696 p.

[19] Foster, M.D. (1960). Interpretation of the Composition of Trioctahedral Micas: United States. Geol. Surv. Prof. Paper 354 (B), 1-146. https://doi.org/10.3133/pp354B

[20] Albuquerque, C.A.R. (1973) Geochemistry of Biotites from Granitic Rocks, Northern Portugal. *Geochimica et Cosmochimica Acta*, **37**, 1779-1802. https://doi.org/10.1016/0016-7037(73)90163-4

[21] Deer, W.A., Howie, R.A. and Zussman, J. (1962) Rock-Forming Minerals, 1 (Ortho and Ring Silicates). Longman, London.

[22] Miller, C.F., Stoddard, E.F., Bradfish, L.J. and Dollase, W.A. (1981) Composition of Plutonic Muscovite: Genetic Implications. *Canadian Mineralogist*, **19**, 25-34.

[23] Ganwa, A.A. (2005) Les granitoïdes de Méiganga: Étude pétrographique, géochimique, structurale et géochronologique. Leur place dans la chaîne panafricaine.

Thèse de doctorat d'Etat, Univ. Yaoundé I, Yaoundé, 162 p.

[24] Henry, D.J. and Dutrow, B.L. (1996) Metamorphic Tourmaline and Its Petrological Implications. *Reviews in Mineralogy and Geochemistry*, **33**, 503-557. https://doi.org/10.1515/9781501509223-012

[25] Ethier, V.G. and Campbell, F.A. (1977) Tourmaline Concentrations in Proterozoic Sediments of the Southern Cordillera of Canada and Their Economic Significance. *Canadian Journal of Earth Sciences*, **14**, 2348-2363. https://doi.org/10.1139/e77-202

[26] Pirajino, F. and Smithies, R.H. (1992) The FeO/(FeO + MgO) Ratio of Tourmaline: A Useful Indicator of Spatial Variations in Granite-Related Hydrothermal Mineral Deposits. *Journal of Geochemical Exploration*, **42**, 371-381. https://doi.org/10.1016/0375-6742(92)90033-5

[27] Galbraith, C.G., Clarke, D.B., Trumbull, R.B. and Wiedenbeck, M. (2009) Assessment of Tourmaline Compositions as an Indicator of Emerald Mineralization at the Tsa da Glisza Prospect, Yukon Territory, Canada. *Economic Geology*, **104**, 713-731. https://doi.org/10.2113/gsecongeo.104.5.713

[28] Kalliomäki, H., Wagner, T., Fusswinkel, T. and Sakellaris, G. (2017) Major and Trace Element Geochemistry of Tourmalines from Archean Orogenic Gold Deposits: Proxies for the Origin of Gold Mineralizing Fluids? *Ore Geology Reviews*, **91**, 906-927. https://doi.org/10.1016/j.oregeorev.2017.08.014

[29] Slack, J.F. (1996) Tourmaline Association with Hydrothermal Ore Deposits. In: Grew, E.S. and Anovitz, L.M., Eds., *Reviews in Mineralogy*, *Vol.* 33, *Boron*: *Mineralogy*, *Petrology*, *and Geochemistry*, Mineralogical Society of America Chantilly, 559-643. https://doi.org/10.1515/9781501509223-013

[30] Deksissa, D.J. and Koeberl, C. (2002) Geochemistry and Petrography of Gold-Quartz-Tourmaline Veins of the Okote Area, Southern Ethiopia: Implications for Gold Exploration. *Mineralogy and Petrology*, **75**, 101-122. https://doi.org/10.1007/s007100200018